Chinese Chemical Letters 37 (2026) 111266

Contents lists available at ScienceDirect

Chinese Chemical Letters

journal homepage: www.elsevier.com/locate/cclet

Modulator-driven structural expansion: From 2D copper coordination polymer to 3D MOF with enhanced proton conductivity

Yongzhen Chen[a,1], Jianxin Ma[c,1], Yuyang Wang[b], Qianqian Liu[b], Yunzuo Cui[b], Weibo Ren[b], Chen Wang[a], Zhong-Min Su[a,c,**], Hong-Ying Zang[b,*]

[a] State Key Laboratory of Supramolecular Structure and Materials, Institute of Theoretical Chemistry, College of Chemistry, Jilin University, Changchun 130021, China
[b] Key Laboratory of Polyoxometalate and Reticular Material Chemistry of Ministry of Education, Faculty of Chemistry, Northeast Normal University, Changchun 130024, China
[c] School of Chemistry and Environmental Engineering, Changchun University of Science and Technology, Changchun 130022, China

ARTICLE INFO

Article history:
Received 30 March 2025
Revised 22 April 2025
Accepted 27 April 2025
Available online 27 April 2025

Keywords:
Modulator
Metal-organic framework
Coordination polymer
Coordination modulation
Proton conduction

ABSTRACT

In this study, we employed sodium hydroxide and 2,6-pyridinedimethanol as modulators to tailor the structure of metal-organic crystals *via* "coordination modulation strategy". Based on this strategy, two copper-based crystalline materials were synthesized *via* hydrothermal synthesis and structurally characterized. Single-crystal X-ray diffraction analysis elucidates that $[Cu_2(\mu_2\text{–OH})(\mu_3\text{–OH})(H_2dcppa)(H_2O)]\cdot H_2O$ (dcppa = 3-(3′,5′-dicarboxyphenoxy)phthalic acid, **CP-1**) exist a kind of $[Cu_4(\mu_2\text{–OH})_2(\mu_3\text{–OH})_2(H_2O)_2]^{4+}$ cluster. Each $[Cu_4(\mu_2\text{–OH})_2(\mu_3\text{–OH})_2(H_2O)_2]^{4+}$ is interconnected in-plane with H_2dcppa ligands, forming a four-directional extended coordination network that ultimately generates a periodically arranged layered architecture. In $[Cu_4(Hdcppa)_2(H_2dcppa)(H_2O)_3]$ (**MOF-1**), there are two types of binuclear copper building blocks, $[Cu_2(H_2O)]^{4+}$ and $[Cu_2(H_2O)_2]^{4+}$, respectively. The adjacent $[Cu_2(H_2O)]^{4+}$ units are interconnected *via* Hdcppa ligands, forming a 1D metal-organic chain. These 1D chains are connected by $[Cu_2(H_2O)_2]^{4+}$ to establish a 2D layer, which is further extended by H_2dcppa ligands to a 3D framework. The successful implementation of this synthetic route further validates the feasibility and effectiveness of combining hydrothermal methods with coordination modulation strategies for the targeted construction of functionalized metal-organic crystals. The proton conductivities (σ) of **CP-1** and **MOF-1** were measured under conditions of 85 °C and 98 % relative humidity (RH), resulting in values of 2.14×10^{-3} and 2.55×10^{-2} S/cm, respectively. This study presents a novel approach to fabricating MOFs as proton conductors through coordination modulation strategy.

© 2026 Published by Elsevier B.V. on behalf of Chinese Chemical Society and Institute of Materia Medica, Chinese Academy of Medical Sciences.

Metal-organic frameworks (MOFs) are a class of crystalline porous materials constructed from inorganic nodes (metal cations/clusters) and multidentate organic ligands, which self-assemble into periodic framework structures [1–3]. MOFs exhibit remarkable chemical diversity, characterized by exceptionally high porosity, large specific surface area, tunable pore structure and designable functionality. Such unique properties make them great candidates in energy, environment, and other fields [4,5]. Many properties of MOFs, such as proton [6,7], electro- [8] conductivity and gas permeability [9] show dependence on pore size and the chemical environment. However, conventional modulator (*e.g.*, NaOH) often drive the assembly of low-dimensional coordination polymers (CPs) rather than porous MOFs, limiting access to advanced functionalities [10,11]. Consequently, precise engineering of anisotropic MOF crystalline architectures has emerged as a critical research focus throughout the past decade.

Multiple synthetic approaches, including microwave-assisted thermal processing, ultrasonication techniques, surfactant-mediated crystallization, and coordination modulation strategies, have been developed for precise regulation of MOF formation processes [12]. Among the prevailing strategies for controlling MOF morphology, the coordination modulation approach has emerged as the most widely adopted methodology. In this process, the competitive interactions between modulators and either organic

* Corresponding author.
** Corresponding author at: State Key Laboratory of Supramolecular Structure and Materials, Institute of Theoretical Chemistry, College of Chemistry, Jilin University, Changchun 130021, China.
E-mail addresses: suzhongmin@jlu.edu.cn (Z.-M. Su), zanghy100@nenu.edu.cn (H.-Y. Zang).
[1] These authors contributed equally to this work.

https://doi.org/10.1016/j.cclet.2025.111266
1001-8417/© 2026 Published by Elsevier B.V. on behalf of Chinese Chemical Society and Institute of Materia Medica, Chinese Academy of Medical Sciences.

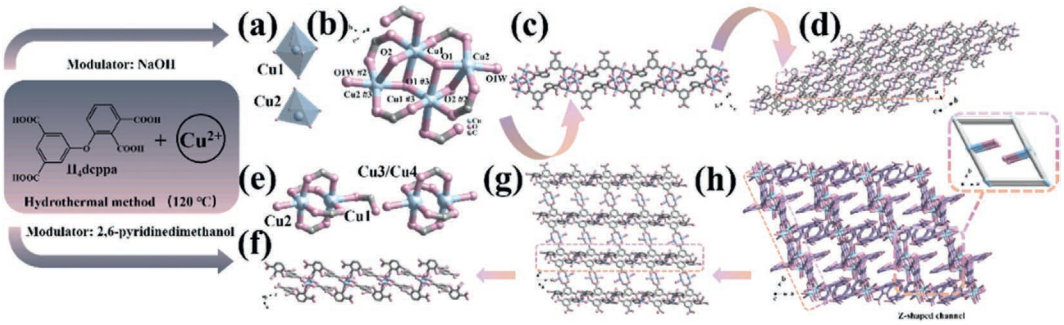


Fig. 1. (a) The coordination mode of Cu1 and Cu2. (b) The structure of $[Cu_4(\mu_2\text{–}OH)_2(\mu_3\text{–}OH)_2(H_2O)_2]^{4+}$ units (The coordinated carboxylic acid groups are added to the structure for clarity). (c) 1D metal-organic chain. (d) metal-organic 2D layer of **CP-1**. (e) The coordination mode of Cu1–4 (The coordinated carboxylic acid groups are added to the structure for clarity). (f) The 1D chain, (g) 2D layer, (h) 3D framework of **MOF-1**.

linkers or inorganic metal clusters serve as critical determinants governing framework assembly. These dynamic competitions ultimately dictate the resultant morphological features, including specific morphologies, crystal sizes and porosity features [13,14]. Furthermore, when employing modulators with acidic/basic functionalities, additional pH-mediated effects may occur within the reaction medium. Such modulation can facilitate precise regulation of protonation/deprotonation equilibria during crystal nucleation and growth stages [15]. Thus, selecting suitable modulators is essential for achieving targeted structural control in MOFs.

After extensive screening and optimization experiments, two modulators (NaOH and 2,6-pyridinedimethanol) were selected as critical synthetic parameters. Using a hydrothermal approach with copper salts as metal nodes and polycarboxylic ligand H_4dcppa as linkers under identical conditions, systematic comparative studies revealed distinct structural outcomes: the introduction of modulator NaOH yielded a two-dimensional layered coordination polymer $[Cu_2(\mu_2\text{–}OH)(\mu_3\text{–}OH)(H_2dcppa)(H_2O)]\cdot H_2O$ (**CP-1**), whereas modulator 2,6-pyridinedimethanol directed the formation of a three-dimensional framework $[Cu_4(Hdcppa)_2(H_2dcppa)(H_2O)_3]$ (**MOF-1**) with ordered channel structures. The test results show that significantly enhanced proton conductivity in the **MOF-1**, with conductivity increasing from 2.14×10^{-3} S/cm (**CP-1**) to 2.55×10^{-2} S/cm (**MOF-1**) at 85 °C and 98 % relative humidity (RH). This finding validates the feasibility of employing novel modulators to control the structural dimensionality and pore characteristics of MOFs, providing an effective methodology for the design of high-performance proton-conductive materials.

Synthesis: **CP-1** and **MOF-1** were prepared at 120 °C under hydrothermal conditions. Among them, the modulator shows an effect on the formation of title materials: For **CP-1**, the pH was adjusted to 3.51 with NaOH. For **MOF-1**, 2,6-pyridinedimethanol was used as the modulator with different deprotonation effects compared to NaOH. It is noteworthy that the competitive binding between modulator 2,6-pyridinedimethanol and primary ligand H_4dcppa induces modifications in the coordination geometry of the latter, thereby resulting in the formation of distinct structural architectures [15]. Therefore, the modulator has a significant impact on the synthesis of title crystals. It is noteworthy that this study is the first to employ 2,6-pyridinedimethanol as the modulator, thereby successfully controlling the structure of the MOFs.

Single-crystal X-ray diffractometry reveals that **CP-1** crystallizes in *P*-1 space group and incorporates tetranuclear copper-oxygen clusters linked with H_4dcppa ligands. Based on the bond valence sum (BVS) calculations and structural characterization, the plate-like **CP-1** consists of two Cu^{II} atoms, one μ_2–OH, one μ_3–OH, one coordinated H_2O molecule, one H_2dcppa ligand and one crystallization water molecule. Additionally, one hydrogen proton was introduced into the formula to balance charge. As demonstrated in Fig. 1a, the Cu1 atoms adopt an octahedral geometry, which coordinated with one μ_2–OH, one μ_3–OH, one coordinated H_2O molecule and three carboxylate groups from three H_2dcppa ligands. The five-coordinated Cu2 atoms defined by one μ_2–OH, one μ_3–OH, one coordinated H_2O molecule and two carboxylate groups from two H_2dcppa ligands. It is observed that a type of $[Cu_4(\mu_2\text{–}OH)_2(\mu_3\text{–}OH)_2(H_2O)_2]^{4+}$ cluster is assembled (Fig. 1b). The carboxylate groups from H_2dcppa ligands are decorated on the clusters forming a 1D tetranuclear copper-based chain (Fig. 1c). The H_2dcppa ligands serve as connectors in the 2D network linking with these 1D chains to continue the structure of **CP-1** (Fig. 1d). Notably, **CP-1** exhibits a 2D layered architecture featuring surface-exposed uncoordinated carboxyl groups.

MOF-1 crystallizes in the *P*-1 space group. On the basis of BVS analysis and structural evaluation, **MOF-1** assembled from four Cu^{II} atoms, two Hdcppa ligands, one H_2dcppa ligand and three coordinated H_2O molecules. To achieve charge balance, a proton was incorporated into the formula. As presented in Fig. 1e, Cu1∼4 display five-coordinated geometry. Among them, the Cu1 atoms coordinate with five carboxylate groups from four Hdcppa ligands and one H_2dcppa ligand. The Cu2 atoms are bonded to one H_2O molecule and four carboxylate groups derived from four Hdcppa ligands. The Cu3 and Cu4 adopt a similar coordination configuration, which exhibit coordination with two H_2O molecules and four carboxylate groups from two Hdcppa ligands and two H_2dcppa ligands.

In **MOF-1**, there are two types of binuclear copper building blocks, $[Cu_2(H_2O)]^{4+}$ and $[Cu_2(H_2O)_2]^{4+}$, respectively. The adjacent $[Cu_2(H_2O)]^{4+}$ units are interconnected *via* Hdcppa ligands, forming a 1D metal-organic chain (Fig. 1f). The $[Cu_2(H_2O)_2]^{4+}$ architectural units act as bridging linkers, connecting these chains to generate a 2D metal-organic layer (Fig. 1g). Ultimately, coordination interactions between H_2dcppa ligands and $[Cu_2(H_2O)_2]^{4+}$ architectural units from the 2D layers lead to the formation of a sTable 3D framework (Fig. 1h). Remarkably, the 3D framework of **MOF-1** contains Z-shaped channels featuring ordered uncoordinated carboxyl groups.

The IR spectra, PXRD patterns, and TG curves for **CP-1** and **MOF-1** are presented in Figs. S1-S3 (Supporting information), with detailed descriptions included in Supporting information, confirming their composition and purity.

Microscopic and scanning electron microscope (SEM) observations reveal that crystals synthesized using different modulators exhibit distinctly different morphologies. As shown in Fig. 2a, **CP-1** displays a light blue, cluster-like structure with an individual crystal plate having a longitudinal dimension of approximately 117 μm (Fig. 2c), whereas **MOF-1** exhibits a dark blue, rectangular block-like morphology (Fig. 2b) with a longitudinal dimension of about 100 μm (Fig. 2d).

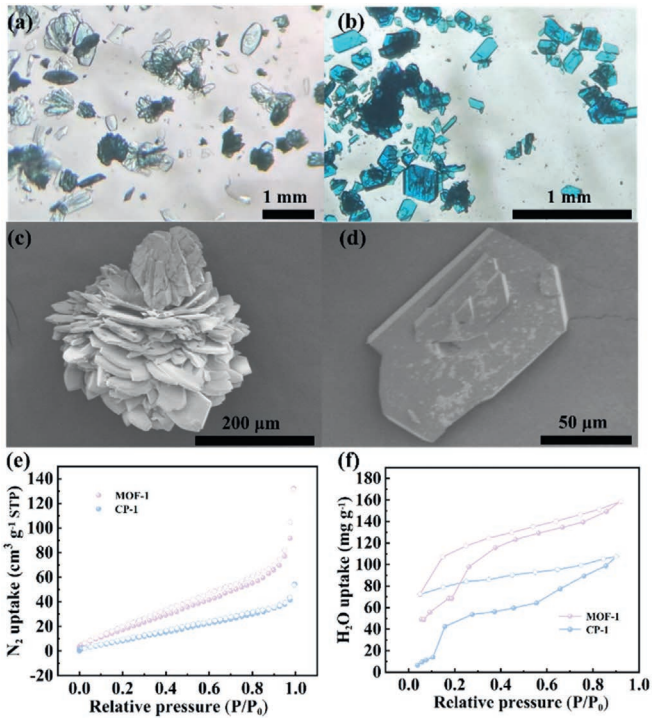


Fig. 2. Optical images of (a) **CP-1** and (b) **MOF-1**. SEM images of (c) **CP-1** and (d) **MOF-1**. (e) BET surface analysis of **CP-1** and **MOF-1**. (f) Water uptake isotherms of **CP-1** and **MOF-1** (measured at 30 °C).

The surface area and porosity of **CP-1** and **MOF-1** were assessed *via* nitrogen adsorption measurements at 77 K. As shown in Fig. 2e, the Brunauer–Emmett–Teller (BET) surface areas of **CP-1** and **MOF-1** were determined to be 54.44 and 132.35 m^2/g, respectively. This indicates that **MOF-1** exhibits a marked advantage in terms of pore structure and specific surface area, further confirming its potential application as a proton conductor [16].

Investigating water uptake in materials is essential for probing proton transport mechanisms, as H_2O molecules serve as key mediators in enhancing conductivity [17,18]. These molecules facilitate the formation of H-bond networks, and the high water uptake enables **CP-1** and **MOF-1** to establish extended H-bond pathways under elevated humidity conditions. As revealed in Fig. 2f ($P/P_0 = 0.95$), **MOF-1** exhibits superior moisture absorption capacity (158.8 mg/g) relative to **CP-1** (107.5 mg/g). Under varying humidity conditions, **CP-1** exhibits enhanced water retention capacity due to hydrogen bonds formed between uncoordinated carboxyl groups on its 2D layered surface and adsorbed water molecules. Compared to **CP-1**, **MOF-1** not only contains abundant ordered carboxyl groups but also features unique Z-shaped hydrophilic water transport channels, thus leading to superior water retention capability [19,20].

Considering the multiple proton hopping sites in **CP-1** and **MOF-1**, combined with the WVA test results, we evaluated their proton conductivity. The proton conductivity of **CP-1** and **MOF-1** were investigated at 25 °C *via* alternating current impedance spectroscopy. As the relative humidity (RH) increased from 70 % to 98 %, the proton conductivity of **CP-1** increased from 1.53×10^{-6} S/cm to 5.13×10^{-6} S/cm, while that of **MOF-1** increased from 3.02×10^{-8} S/cm to 1.16×10^{-3} S/cm (Fig. 3a). These results demonstrate that **CP-1** and **MOF-1** exhibit high humidity dependence. At 25 °C under varying humidity conditions, **MOF-1** shows a more pronounced variation in proton conductivity. Furthermore, as the relative humidity gradually increases, **MOF-1** displays significantly superior proton-conductive performance compared to **CP-1**. This enhancement is primarily attributed to the abundance of water molecules under high-humidity conditions, which facilitates the formation of efficient proton transport pathways through proton carriers within the hydrophilic channels of **MOF-1**, thereby improving proton conduction efficiency [21–25].

In addition to variations in relative humidity, temperature significantly influences the migration rate of proton carriers, thereby impacting the proton conductivity of the crystalline framework. Variable-temperature tests were performed on **CP-1** and **MOF-1** under 98 % RH, covering a temperature range of 35–85 °C with 10 °C intervals and 1-h equilibration at each step. For **CP-1**, the proton conductivity increased from 7.06×10^{-5} S/cm to 2.14×10^{-3} S/cm (Figs. S4 and S5 in Supporting information). **MOF-1** similarly exhibited an increasing trend (Fig. 3b), with values of 1.21×10^{-3} S/cm to 2.55×10^{-2} S/cm. Notably, elevated temperatures enhance the proton conductivity of **CP-1** and **MOF-1**, attributed to faster proton movement within the structures. **MOF-1** exhibits a proton conductivity of 2.55×10^{-2} S/cm under 98 % RH and 85 °C. This superior performance is attributed to its unique Z-shaped hydrophilic channels, which facilitate directional and rapid proton transport. Remarkably, its conductivity rivals that of many reported crystalline proton conductor (Table S5 in Supporting information). The stability of proton conductivity in **CP-1** and **MOF-1** was investigated. To assess this critical property, **CP-1** and **MOF-1** were exposed to 85 °C, 98 % RH. Over a 24-h continuous operation period, their proton conductivity exhibited negligible variation (Fig. 3c and Fig. S6 in Supporting information), demonstrating exceptional operational durability. Importantly, comparative analysis of pre- and post-test IR spectra and PXRD patterns (Figs. 3d and e, Figs. S7 and S8 in Supporting information) revealed preserved structural integrity with no detectable framework degradation, indicating their structural stability under conditions of elevated temperature and humidity. The time-dependent current profiles for **CP-1** and **MOF-1** were measured using the Hebb-Wagner direct current polarization method [26,27]. As depicted in Fig. S9 (Supporting information), a constant voltage of 0.1 V was applied, and the resulting current curves revealed values of about 0.17 and 0.73 nA for **CP-1** and **MOF-1**, respectively, with corresponding resistances of 5.9×10^8 and 1.3×10^8 Ω. These results confirm their dominant proton conduction behavior over electronic conduction.

The conduction mechanisms of **CP-1** and **MOF-1** were analyzed *via* Arrhenius plots. As depicted in Fig. 3f and Fig. S10 (Supporting information), the derived activation energy (E_a) values (0.57 eV for **MOF-1** and 0.67 eV for **CP-1**) surpass the 0.4 eV threshold, unambiguously indicating adherence to the Vehicle mechanism [28–30]. Fig. 4 illustrates the proton transport pathways under this mechanism, where protons migrate through H_3O^+ complexes formed with mobile water molecules. In such systems, freely diffusing lattice water molecules serve as dynamic proton carriers, enabling rapid directional transport [31,32]. The enhanced proton mobility in **CP-1** arises from carboxyl-containing ligands and water species (coordinated or lattice) within its 2D layered structure, which form a hydrogen-bonding network. Within this network, adsorbed water molecules promote adjacent proton migration, thereby providing continuous pathways for efficient proton conduction. **MOF-1** achieves exceptional proton conduction through its 3D framework featuring Z-shaped channels enriched with water molecules and uncoordinated carboxyl groups. These components collectively establish a hydrogen-bonding network that directs protons along ordered pathways, resulting in rapid proton transport.

In summary, we have effectively synthesized two copper-based crystalline materials. The transformation of coordination polymer (**CP-1**) into metal-organic framework (**MOF-1**) was successfully achieved through a coordination modulation strategy. The proton conductivity of **CP-1** and **MOF-1** was evaluated at 85 °C and 98 % RH, yielding values of 2.14×10^{-3} and 2.55×10^{-2} S/cm, re-

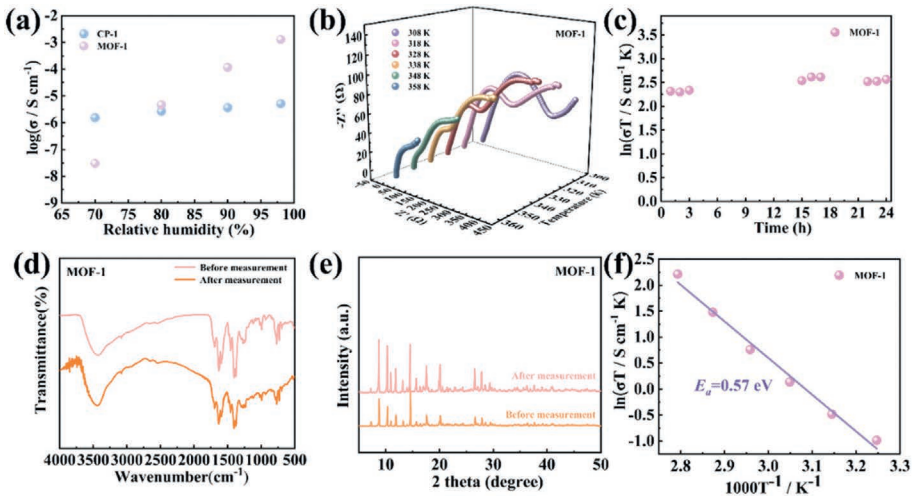


Fig. 3. (a) RH-dependent proton conductivity of **CP-1** and **MOF-1** at 25 °C. (b) Nyquist plots of **MOF-1** from 35 °C to 85 °C. (c) Proton conductivity stability of **MOF-1** at 85 °C and 98 % RH. (d) IR spectrum and (e) PXRD patterns of **MOF-1**. (f) Arrhenius plots and linear fitting of **MOF-1**.

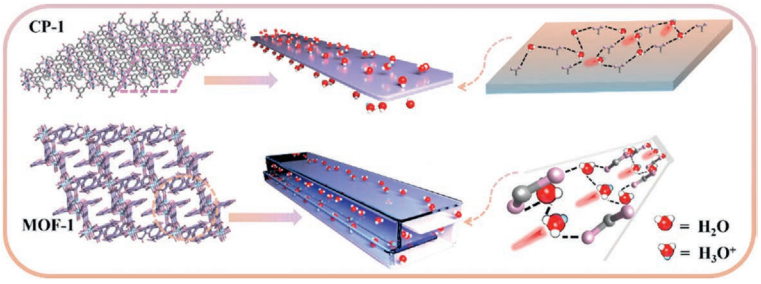


Fig. 4. Schematic illustrations of proton-conducting pathways in **CP-1** and **MOF-1**.

spectively. The exceptional proton conductivity of **MOF-1** originates from two synergistic factors: (1) The 3D framework incorporates Z-shaped proton-conducting channels, which facilitate directional proton migration along ordered pathways; (2) These channels, densely populated by water molecules and uncoordinated carboxyl groups, collectively establish a continuous hydrogen-bonding network to enable efficient proton hopping. Further study on using this strategy to design other types of MOFs with special pore channels is currently underway.

Declaration of competing interest

The authors declare that they have no known competing financial interests or personal relationships that could have appeared to influence the work reported in this paper.

CRediT authorship contribution statement

Yongzhen Chen: Writing – original draft, Validation, Supervision, Software, Formal analysis, Data curation, Conceptualization. **Jianxin Ma:** Formal analysis, Data curation, Conceptualization. **Yuyang Wang:** Data curation, Conceptualization. **Qianqian Liu:** Conceptualization. **Yunzuo Cui:** Data curation. **Weibo Ren:** Software. **Chen Wang:** Data curation. **Zhong-Min Su:** Writing – review & editing. **Hong-Ying Zang:** Writing – review & editing.

Acknowledgments

This work was supported by the National Natural Science Foundation of China (Nos. 22322102, 21471028, 21673098, 21671036, 22271023), the Fundamental Research Funds for the Central Universities Excellent Youth Team Program (No. 2412023YQ001), Natural Science Foundation of Jilin Province (No. 20200201083JC), Jilin Provincial Education Department (No. JJKH20201169KJ), the Fundamental Research Funds for the Central Universities (Nos. 2412015KJ012, 2412017BJ004), and the support of the Jilin Provincial Department of Education.

Supplementary materials

Supplementary material associated with this article can be found, in the online version, at doi:10.1016/j.cclet.2025.111266.

References

[1] I.E. Khalil, J. Fonseca, M.R. Reithofer, et al., Coord. Chem. Rev. 481 (2023) 215043.
[2] H.R. Tian, Zhang Z, S.M. Liu, et al., Green Chem. 22 (2022) 7513–7520.
[3] B. Mohanty, S. Kumari, P. Yadav, et al., Coord. Chem. Rev. 519 (2024) 216102.
[4] L.X. Shi, Y.H. Shi, Y.Q. Xu, et al., J. Environ. Chem. Eng. 11 (2023) 111468.
[5] Y.X. Wang, Y. Lu, W.S. Zhang, et al., Polyoxometalates 1 (2022) 9140005.
[6] S. Srivastava, S.P. Shet, S.S. Priya, et al., Int. J. Hydrog. Energy 47 (2022) 15820–15831.
[7] Y.F. Dong, S.J. Zhong, Y.H. He, et al., Chin. Chem. Lett. 35 (2024) 109261.
[8] J.S. Luo, X. Jia, C.T. Ren, Matter 5 (2022) 772–774.
[9] K. Nath, A. Ahmed, D.J. Siegel, et al., J. Am. Chem. Soc. 144 (2022) 20939–20946.
[10] M. Boone, F. Artizzu, J. Goura, et al., Coord. Chem. Rev. 501 (2024) 215525.
[11] G. Sharma, A. Verma, T. Wang, et al., Coord. Chem. Rev. 519 (2024) 216120.
[12] F. Bigdeli, M.N.A. Fetzer, B. Nis, et al., J. Mater. Chem. A 11 (2023) 22105–22131.
[13] H.L. Guo, Y.Z. Zhu, S.L. Qiu, et al., Adv. Mater. 22 (2010) 4190–4192.
[14] T. Tsuruoka, S. Furukawa, Y. Takashima, et al., Angew. Chem. Int. Ed. 121 (2009) 4833–4837.
[15] F.L. Wang, H.L. Guo, Y.M. Chai, et al., Microporous Mesoporous Mat. 173 (2013) 181–188.
[16] P.Y. You, K.M. Mo, Y.M. Wang, et al., Nat. Commun. 15 (2024) 194.

[17] R. Keloth, O.A. Obewhere, K. Acurio-Cerda, et al., ACS Sustain. Chem. Eng. 13 (2025) 4132–4147.
[18] K. Zhang, L. Wu, K. Gong, et al., Angew. Chem. Int. Ed. 64 (2025) e202421444.
[19] X.M. Li, J.C. Jia, D.T. Yang, et al., Chin. Chem. Lett. 35 (2024) 108474.
[20] J.D. Núñez, A.M. Benito, S. Rouzière, et al., Chem. Sci. 8 (2017) 4987–4995.
[21] Y.Y. Ma, J. Liu, W.X. Yan, et al., Microporous Mesoporous Mater. 367 (2024) 112974.
[22] R.M. Shi, Z.Q. Zhang, F. Yang, et al., Microporous Mesoporous Mater. 343 (2022) 112192.
[23] H. Wu, F. Yang, X.L. Lv, et al., J. Mater. Chem. A 5 (2017) 14525–14529.
[24] J.L. Li, J.H. Wang, F. Shui, et al., Chin. Chem. Lett. 34 (2023) 107917.
[25] D.M. Cheng, Z.X. Gao, W.W. Wang, et al., Polyoxometalates 2 (2023) 9140019.
[26] T. Miruszewski, K. Dzierzgowski, P. Winiarz, et al., J. Mater. Chem. A 10 (2022) 7218–7227.
[27] T. Miruszewski, R. Strandbakke, K. Dzierzgowski, et al., J. Mater. Chem. A 12 (2024) 13488–13497.
[28] J. Lee, D.W. Lim, S. Dekura, et al., ACS Appl. Mater. Interfaces 11 (2019) 12639–12646.
[29] W.B. Ren, B. Li, Y.Z. Cui, et al., Inorg. Chem. 63 (2024) 20307–20313.
[30] L. Zhang, Z. Liu, C.X. Yang, et al., ACS Nano 16 (2022) 13771–13782.
[31] H.Y. Sun, S.H. Sun, B. Hu, et al., Inorg. Chem. Front. 7 (2020) 1699–1703.
[32] B.J. Kim, S.H. Park, M.L. Díaz-Ramírez, et al., Chem. Commun. 61 (2025) 3582–3600.